We are IntechOpen, the world's leading publisher of Open Access books Built by scientists, for scientists

4,800
Open access books available

122,000
International authors and editors

135M
Downloads

Our authors are among the

154
Countries delivered to

TOP 1%
most cited scientists

12.2%
Contributors from top 500 universities

CLARIVATE ANALYTICS BOOK CITATION INDEX INDEXED

WEB OF SCIENCE™

Selection of our books indexed in the Book Citation Index in Web of Science™ Core Collection (BKCI)

Interested in publishing with us?
Contact book.department@intechopen.com

Numbers displayed above are based on latest data collected.
For more information visit www.intechopen.com

23

3D Network SiC-Metals Composites for Heavy Duty Brake Applications

Hongqiang Ru, Jingyang Li and Wei Wang
School of Materials and Metallurgy, North Eastern University, Shenyang China

1. Introduction

A critical component of high-speed trains is their braking systems. A key technology of a braking system is the braking material. Its primary function is to dissipate mechanical energy by converting it into heat during the braking process without experiencing damages in structure and deterioration in property.

Currently, the most commonly used brake materials for high-speed trains of 200~300 km/hour are copper matrix powder metallurgy materials composed by base metal Cu, Sn and Zn and additives Fe, Ni, Mo and graphite (Desplanques et al., 2001). These materials have various advantages such as stable friction coefficient, lower noise compared to iron shoe materials, high thermal conductivity and well running-in characteristic (Zhang et al., 2010) and (Wahlström et al., 2010). However, with increasing the speed to 380 km/hour, these materials suffer from several problems including adhesion, over abrasion, fatigue fracture and flake spalling. These materials become inadequate to withstand 30 MJ of braking energy during the braking process in emergency situations (Guérin et al., 1997).

Therefore, it is necessary to develop new brake materials of improved performances. The development of these materials is critical for the success of the technology of high-speed trains. The success of the project is of high technical significance.

To meet the request for brake material application for speeds above 350 km/hour, main properties of the brake material need to satisfy the following requirements (Tirovic et al., 2001):

1. Heat capacity above 500 J/kg.K;
2. Thermal conductivity above 45 W/m·K;
3. Crushing strength above 280 MPa;
4. Bending strength above 70 MPa;
5. Average friction coefficient 0.35 and the vibration below 20%;
6. Abrasion below 2×10^{-3} $cm^3/MJ \cdot cm^2$;
7. Withstand heat energy above 30 MJ during braking.

The current copper matrix braking materials are able to meet all the above except requirements (1) and (7). Their heat capacities are 390 J/kg.K. Moreover, they cannot dissipate 30 MJ. Generally, at 22 MJ, their surface temperature may reach 1100°C, above the melting point of copper (Bauer&Li, 2005). To solve the problem, an option is to introduce second phase materials of high melting points and high heat capacities into the copper

matrix. These second phase materials with higher heat capacities will absorb more heat energy than copper, thus lower the surface temperature of the composite.

Silicon carbide (SiC) is widely studied for its high temperature stability, high thermal conductivity, high hardness and high heat capacity. Its melting point is above 2600°C, and the thermal conductivity is 16.7 W/m·K. Moreover, its heat capacity is 712 J/kg.K at 373 K (Lide, 2009), which increases with increasing temperature. These properties present SiC the possibility as potential additive to copper based braking material.

The concept of the new braking material is a copper matrix-SiC 3D network composite, of which the volume fraction of SiC is 40%. It is to be formed by infiltrating Cu into SiC performs. The interpenetrating composites are expected not only to preserve the properties of stable friction coefficient, low noise, high thermal conductivity and good running-in characteristics of copper, but also to ensure the mechanical and thermal properties of bending strength, crushing strength, heat capacity, as well as thermal conductivityso to overcome the problems of flaking, over abrasion and yielding. It is also intend to introduce SiC into other metal matrices, including pure iron, cast steel and stainless steel.

This chapter presents the 3D SiC ceramics network-metals composites brake materials, including the preparation procedure, the discovery of SiC-metals interfaces, the experimental evidences and discussions of reaction, as well as the brake properties of this new concept material. This chapter is divided into Three sections. The first section introduces the 3D SiC-copper composites. The second section introduces the 3D-SiC-5120 steel composites. The third section introduces the brake properties of these 3D SiC-metals composites materials.

2. SiC-Cu composites

2.1 Composites preparation

The experimental work involved the preparation of SiC skeleton. In the present study, the 6H-SiC and SiC powder have been used for preparation of SiC skeleton and sintered to SiC skeleton preform. The experiment involved the preparation of SiC-Cu composites. The method, which patented in China (Ru et al., 2006), is to cast Cu into the SiC skeleton in a special furnace at 1160 by pressure, caused by pressure difference between pressured gas and vacuum. The Cu interpenetrated the SiC skeleton and formed the composites. After the preparation, the SiC-Cu was sliced into 10mm×10mm×5mm pieces and polished metallographically. Microstructural characterization of the reaction zone was carried out by the optical microscope and the scanning electron microscopy (SEM), and the production of the solid reaction was identified by means of X-ray diffraction (XRD).

2.2 Microstructure

It is observed that the Cu in the present investigation reacted with the SiCn and develop a variety of phases close to the reaction zone (Kang&Kang, 2006). The secondary electron image and the composition profile obtained by the SEM are shown in Figure 1. The micrograph shows a nice contact between SiC and reaction zone. However, there is a gap in the interface between the SiC and the reaction zone. The gap may be due to the different thermo expansion coefficient. Meanwhile, the dark phase, which is shown in the secondary electron image, is essentially SiC particle picked up during the polish procedure from the polish paper. The sequence of reaction layers formed in the SiC-Cu system consists of SiC reaction zone, random carbon precipitation zone, regulative carbon precipitation zone and

metal reaction zone, shown as Figure 1. (b), from section I to section IV. In section I, SiC decomposed to Carbon and Silicon. And the Silicon, which has good affinity with Cu, formed the compound as Cu_4Si, identified by XRD and EDS (Figure 2 and Figure 3). Meanwhile, the carbon failed to form the solid solution with Cu, according to the binary phase diagram, diffused against the SiC, and precipitated in the section II and section III. With the increasing distance from the SiC terminal to the precipitation location, the carbon scale increased and the shape transformed from the anomaly in the section II to the regulative round in the section III.

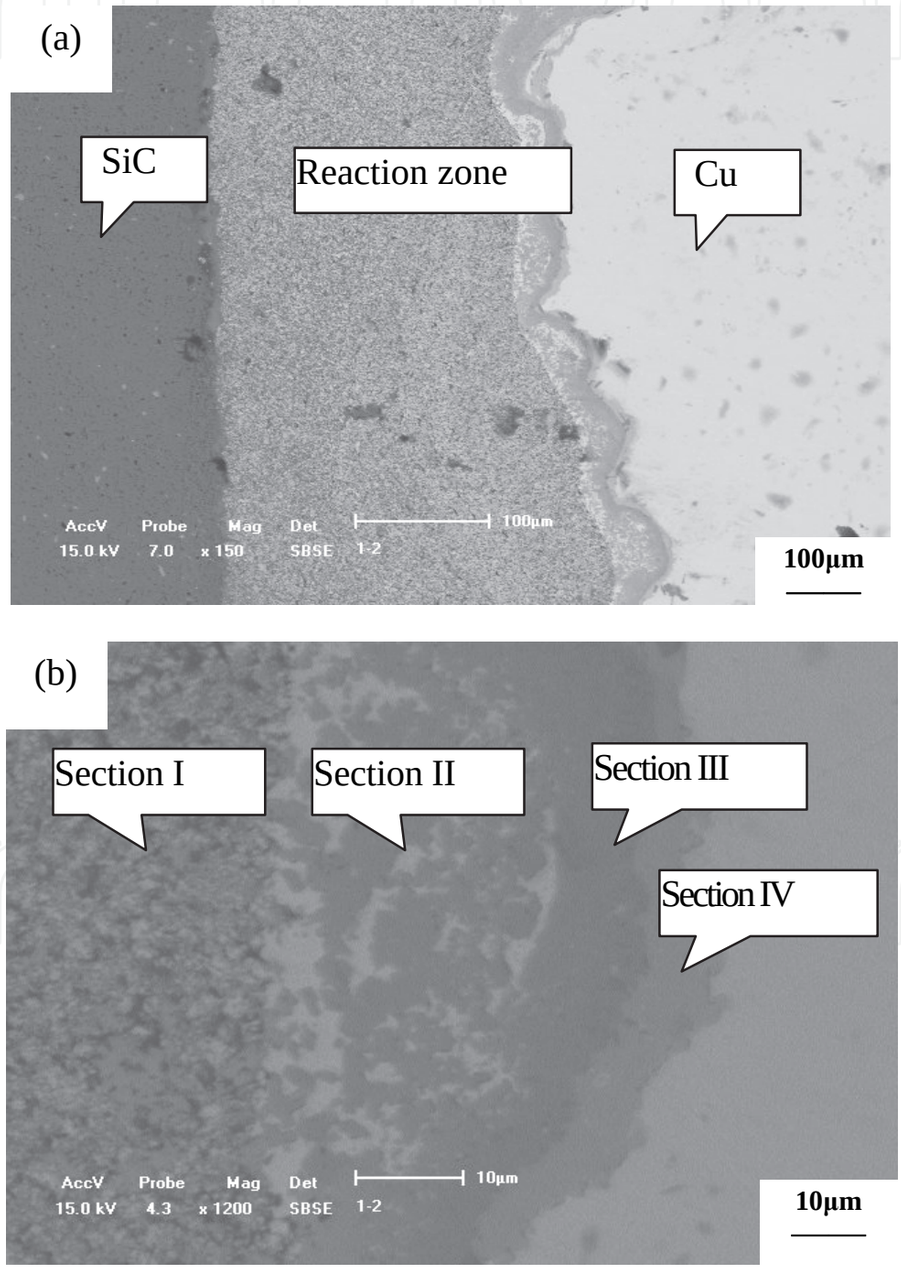

Fig. 1. Secondary electron image of the cross section of the SiC-Cu composites

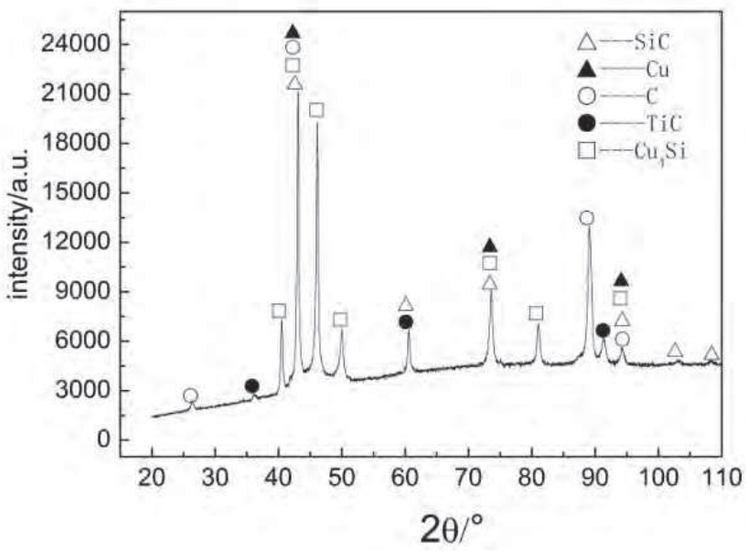

Fig. 2. The XRD patern of SiC-Cu composites

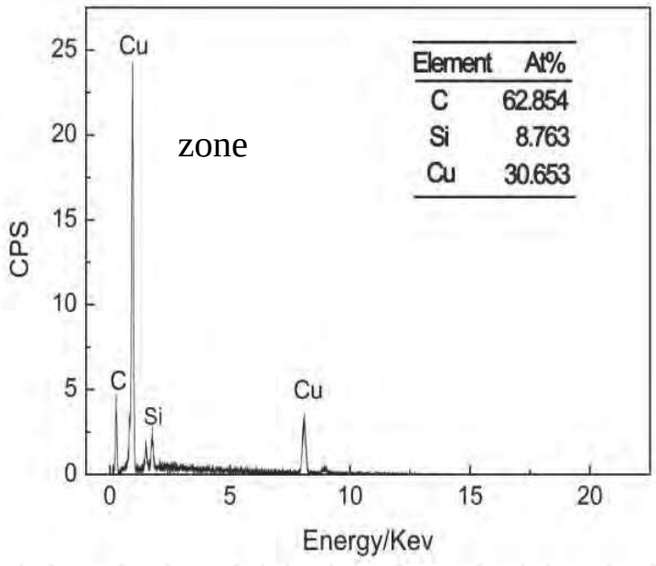

Fig. 3. The EDS patern of SiC-Cu reaction interface

The formation of the interface of SiC-Cu is co-operated by the liquid reaction during the casting process, the solid reaction during the cooling process and the diffusion of the elements. The equation 1 and 2 shows the main reaction:

$$SiO_2(s)+Cu(l)\rightarrow Cu4Si(s)+Cu_2O(s) \quad (1)$$

$$SiC(s)+Cu(l)\rightarrow Cu_4Si(s)+C(s) \quad (2)$$

At the beginning of the whole process, the silicon carbide skeleton, pre-oxidized, was eroded by the copper liquid. The SiO_2 film was crushed, decomposed into Si, formed Cu_4Si

with copper, and Oxygen, formed copper oxides and diffused against the SiC. As the copper liquid contacted with the SiC, the reaction started cosmically. Since the copper was superfluous in this certain reaction, the products and the degree of the reaction were controlled by the speed of the silicon carbide decomposition. Basically, the SiC could not decompose in the environment of 1160°C, but the presence of the copper supply the dynamic force to the SiC system (Rado&Drevet, 2000). The Si had the great affinity with the copper, forming Cu-Si compound, while the carbon failed to solute in the copper matrix and precipitated as the graphite phase. According to the previous research (Zhang, 2008), the precipitation of the carbon was oblige to meet the requests as follow: (1) the metal has greater affinity with the silicon more than the carbon; (2) the concentration of the metal atoms has to be heavy so as to supply the force to decompose the SiC; (3) the carbon has the light solubility in the metal matrix. In this paper, the SiC-Cu system happened to meet the requests above.

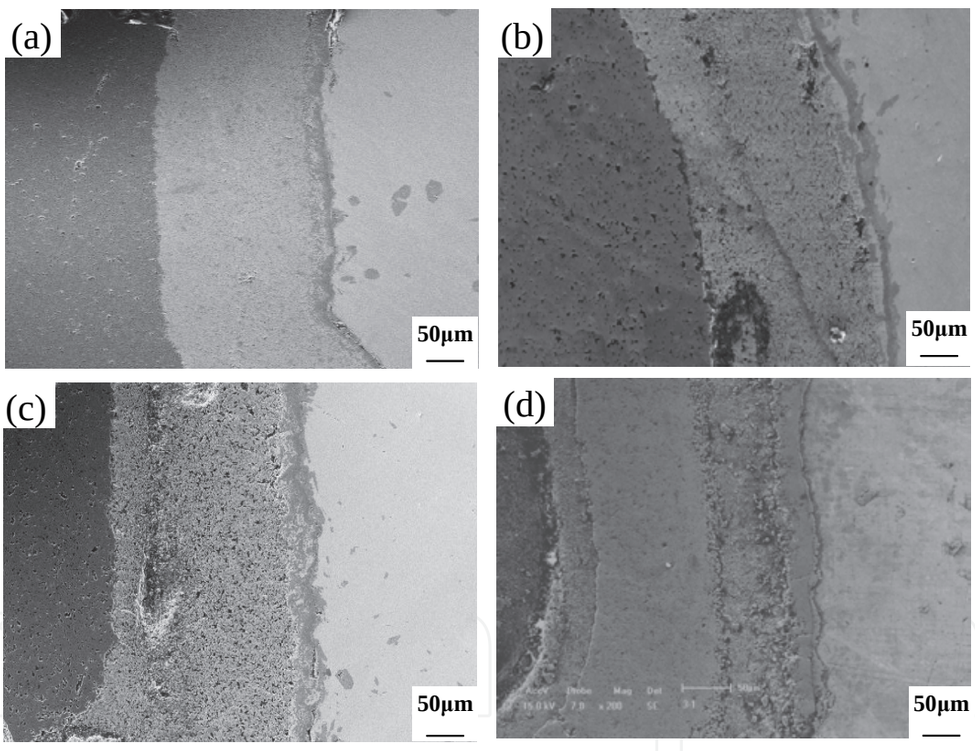

Fig. 4. The microstructure of interface region after heat treatment
(a)30min; (b)60min; (c)90min; (d)120min

In order to make clear the mechanism of the solid reaction around the interface in the SiC system, this paper has research the diffusion behavior and calculated the diffusion coefficient as well. As the Figure 4 shows, the section II of the interface was heat treated, lasting 30, 60, 90 and 120 minutes respectively. For the reason that the band of the section II was narrow, this paper chose this section so as to control the precision and to observe the change of the morphology. The distance from the copper matrix to the section II was 30μm,

measured. And the content of the copper in the section II in the original specimen and the heat treated ones was shown in the table.1.

0 min	30min	60min	90min	120min
52.7%	57.4%	62.1%	66.0%	70.3%

Table 1. Content of Cu in the section II after different heat treatment time

Based on the Fick's law and the equation of semi-infinite objects (Equation 3), this paper substituted the initial condition: C_S=1, C_1=0, and drew the equation 4.

$$C=C_S-(C_S-C_1)\mathrm{erf}(\frac{x}{2\sqrt{Dt}}) \tag{3}$$

$$C=1-\mathrm{erf}(\frac{x}{2\sqrt{Dt}}) \tag{4}$$

After substituted the value as x=30μm, C=52.7% while t=t, C_1=57.4% while t_1=t+1800, C_2=62.1% while t_2=t+3600, C_3=66.0% while t_3=t+5400, and C_4=70.3% while t_4=t+7200 respectively, the diffusion coefficient was calculated: $D_1=2.85\times10^{-14}$ $m^2 \cdot s^{-1}$, $D_2=2.31\times10^{-14}$ $m^2 \cdot s^{-1}$, $D_3=2.79\times10^{-14}$ $m^2 \cdot s^{-1}$, and $D_4=3.09\times10^{-14}$ $m^2 \cdot s^{-1}$. The average one was $D=2.76\times10^{-14}$ $m^2 \cdot s^{-1}$.

3. SiC-5120 Steel composites

3.1 Composites preparation

A SiC-steel composite was created using a porous SiC network preform and a low alloy 5120 steel of the composition as given in Table 2. To create the composite, SiC powder was first prepared into aqueous slurry. A porous polyurethane block of 10×50×100 mm in external dimension was used as a template to produce SiC preform. The template was submerged into the SiC slurry before taken out to dry at room temperature for 24 hours to form the SiC green pattern, which was then sintered in vacuum at 2000 °C to create the porous SiC preform. The SiC preform was preheated to 450 °C in vacuum prior to steel infiltration. Ingot of 5120 steel was melted in a vacuum furnace at 1650 °C and the molten steel was then poured into the pre-heated SiC preform for infiltration. The infiltrated composite was allowed to solidify and cool down naturally in the vacuum furnace.

	C	Cr	Si	Mn	Fe
5120 steel	0.17~0.24	0.70~1.00	0.17~0.37	0.50~0.80	Balance

Table 2. 5120 steel composition in weight percentage

3.2 Microstructure of composites

Figure 5 shows optical micrographs of the samples of the experiment. Micrograph (a) shows the SiC preform before steel infiltration. The pores are spherical, interconnected and uniform in size and distribution, The average pore diameter is 3 mm and the average pore

wall thickness is ~1 mm. The porosity of the SiC preform created was 15 vol%. Micrograph (b) shows the composite sample after the molten steel infiltration. The dark contrast is the SiC preform and the lighter contrast is the infiltrated 5120 steel.

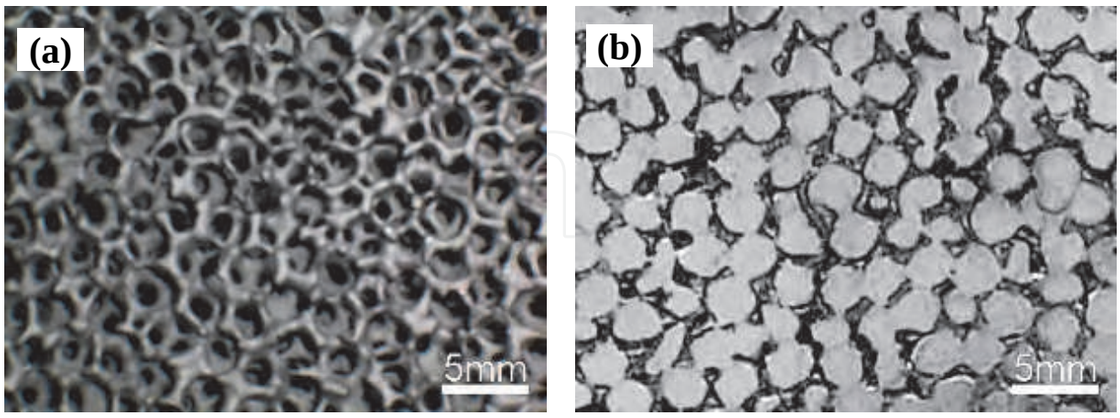

Fig. 5. Optical micrographs of (a) SiC skeleton preform and (b) SiC/20Cr composites sample.

Figure 6 shows detailed microstructures of the SiC/5120 steel composite. Micrograph (a) is an optical image showing different microstructural sections of the composite. The

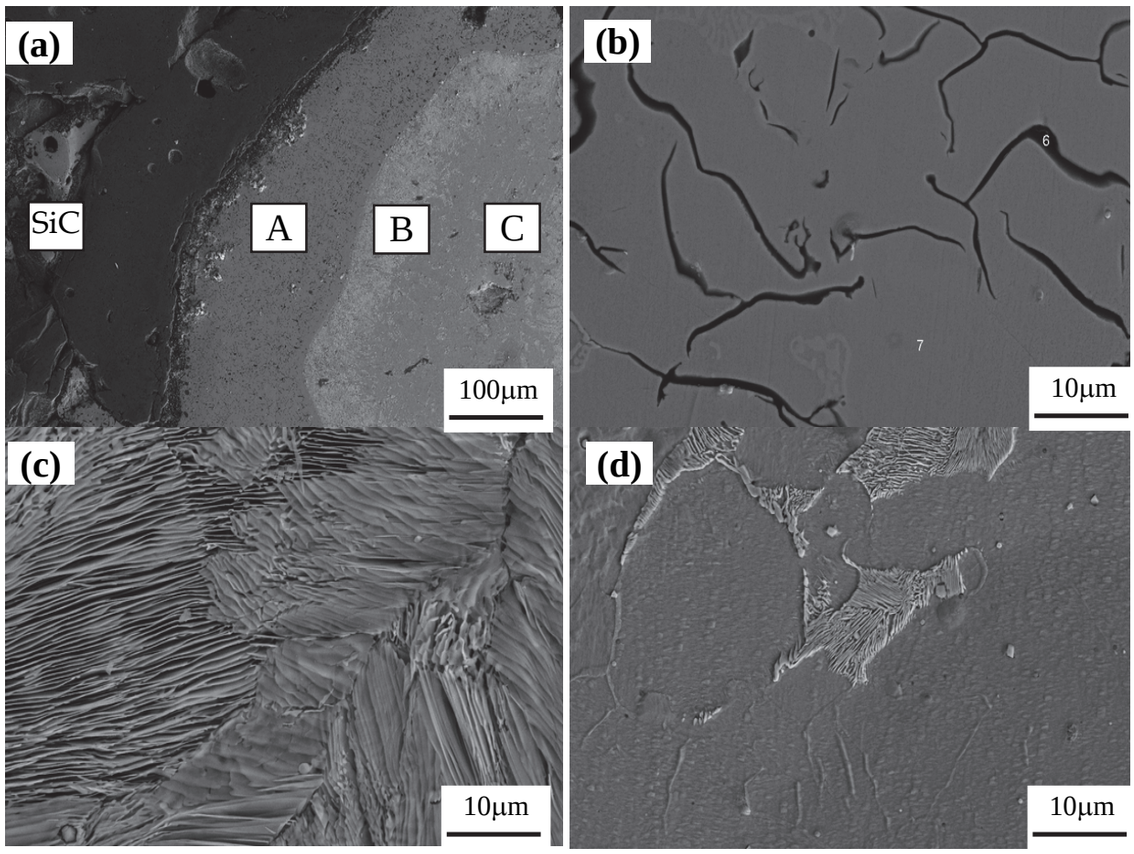

Fig. 6. Microstructures of SiC-5120 steel composite showing different section

microstructure is seen to contain four distinctive sections, labelled A, B, C and SiC. The average width of section A was 230 μm and the average width of section B was 150 μm. Micrograph (b) shows an SEM image of the structure in section A. The structure contains ferrite Fe(Si) solid solution matrix and graphite rosette flakes. EDS analysis of the matrix phase showed Si content of 13 at%, corresponding to the α1-Fe(Si) ferrite phase in the bindary Fe-Si system, according to the Fe-Si phase diagram. The volume fraction of graphite is ~8 vol%, estimated by image analysis using ImageJ software. Micrograph (c) is an SEM image of the structure in section B. The structure is pure pearlite. Microhgraph (d) is an SEM image of the structure in section C. It contains a continuous ferrite matrix and scattered colonies of pearlite. The volume fractions of the two structures are determined by means of image analysis to be 75 vol.% ferrite and 25 vol.% pearlite. The total C content in this region may be estimated to be 1 at% based on the volume fractions. It is also evident that a narrow gap of ~40 μm in width existed between SiC and region A. This is caused by the solidification shrinkage of the steel and the difference in thermal expansion coefficients between SiC and the steel, which are 2.98×10^{-6}/°C and 1.5×10^{-5}/°C, respectively.

Figure 7 shows XRD spectrum of the SiC/5120 steel composite. The peaks are fully indexed to SiC and α-Fe(C) ferrite and/or α1-Fe(Si) ferrite. The α-Fe(C) ferrite has a bcc structure and the α1-Fe(Si) ferrite has a DO3 structure, with very similar lattice parameters [21]. Their fundamental diffraction peaks practically overlap on the spectrum. Superlattice diffraction peaks for the DO3 phase are not observed. The lattice constant of the bcc α-Fe(C) ferrite is determined to be a=0.286 nm, or a=0.567 nm for the DO3 α1-Fe(Si). Graphite and cementite (in pearlite) were not detected by XRD, because of their low volume fractions, which are about 0.8 vol.% and 0.9 vol.% in the sample.

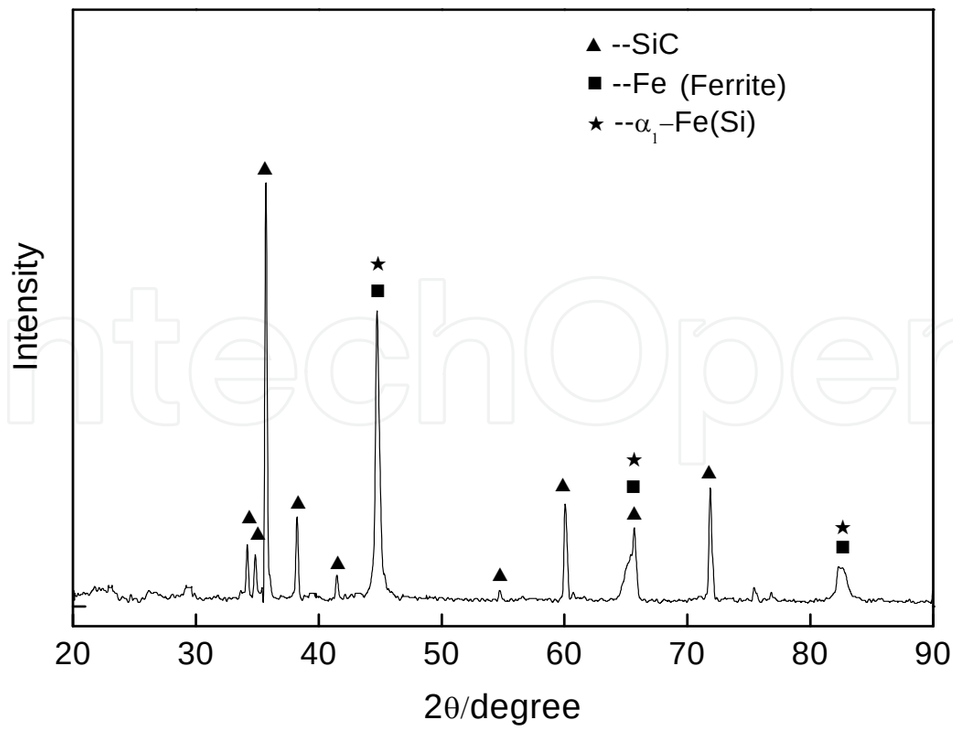

Fig. 7. X-ray diffraction pattern at room temperature of the SiC/5120 composite

4. Brake properties of SiC-5120 steel and SiC-copper composites

Stable friction coefficient guarantees the security of the brake material application. 3D SiC network-metals composite brake material could afford stable friction coefficient. For example, SiC-steel and SiC-copper sets (SiC-steel brake disc with SiC-copper pad) could keep the friction coefficient above 0.3 stably. Abrasion is another key element in evaluating the brake materials. Lower abrasion could guarantees the longer duration of the brake materials application. In SiC-steel and SiC-copper sets (SiC-steel brake disc with SiC-copper pad), the abrasion of SiC-steel composite is no more than 1.2μm every brake action, while the abrasion of SiC-copper composite is no more than 1.8μm.
Figure 8(a) shows the variation of acceleration with same brake pressure and various initial rolling speed, whereas Figure 8(b) shows the variation of acceleration with various brake pressure and same initial rolling speed.

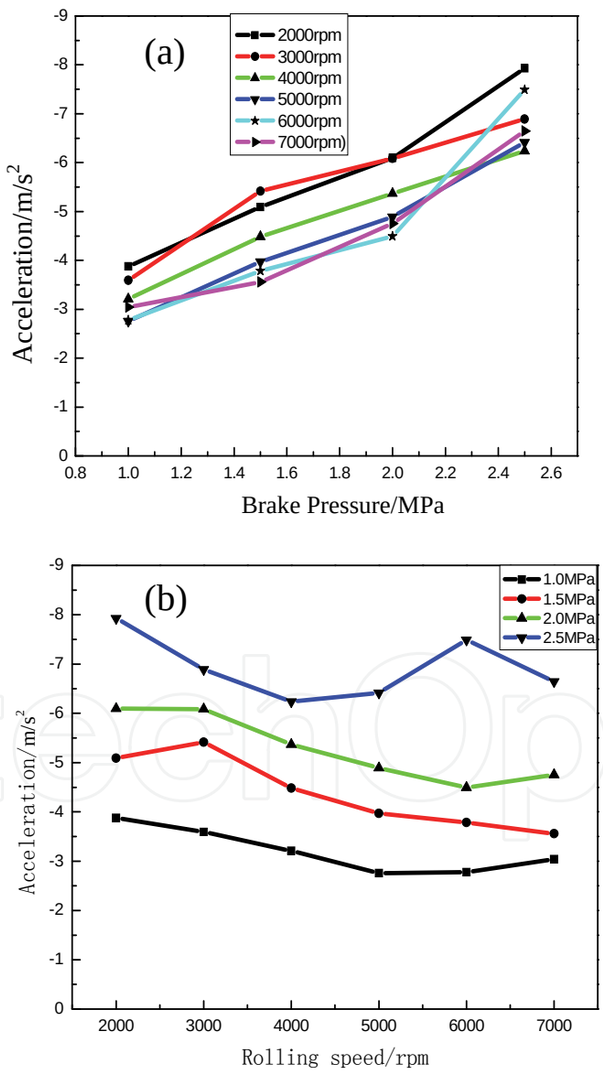

Fig. 8. The relation between the braking acceleration and the brake pressure as well as the rolling speed

It can be seen that under the same rolling speed, the with the increasing brake pressure, the acceleration is ascending, while under the same brake pressure, the acceleration trends stable. For that the more brake pressure, the shorter brake duration, leads to the more acceleration. On the contrary, the more rolling speed, the more brake duration, results in the lower acceleration.

Figure 9(a) shows the friction coefficient variation with the various pressures, whereas Figure 9(b) shows the friction coefficient variation with the same pressure. In lower rolling speed situations (2000 rpm, 3000 rpm and 4000 rpm), the average friction coefficient goes down with the increasing brake pressure, while in higher rolling speed situations (5000 rpm, 6000 rpm, and 7000 rpm), the average friction coefficient ascends after the short descending. Generally, friction coefficient is inversely proportional to brake pressure, so that friction coefficient decrease with the increasing pressure.

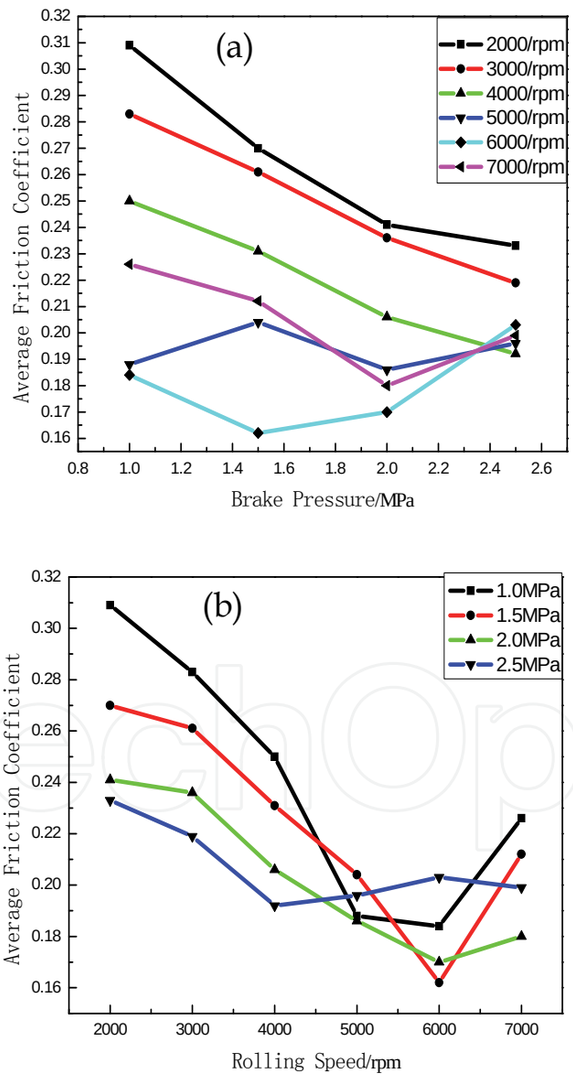

Fig. 9. The relation between the average friction coefficient and the brake pressure as well as the rolling speed

However, in higher rolling speed situations, the mechanism of abrasion is adhesive wear as the main, instead of abrasive grain abrasion as the main. The more brake pressure, the more adhesive wear leading to the more surface damage on the brake material, the less actual friction area. Moreover, the friction coefficient is inversely proportional to actual friction area. The average friction coefficient is increased by the factors described above.

The friction coefficient stability, also known as fluctuation range of friction coefficient, is the value after average friction coefficient subtracted by the maximum friction coefficient.

$$\Delta\mu = \mu_{\max} - \overline{\mu} \tag{5}$$

It is obvious that the less fluctuation range of friction coefficient, the more stable of friction coefficient.

Figure 10(a) shows the variation of friction coefficient stability with various rolling speed while Figure 10(b) shows the variation of friction coefficient stability with various brake pressure.

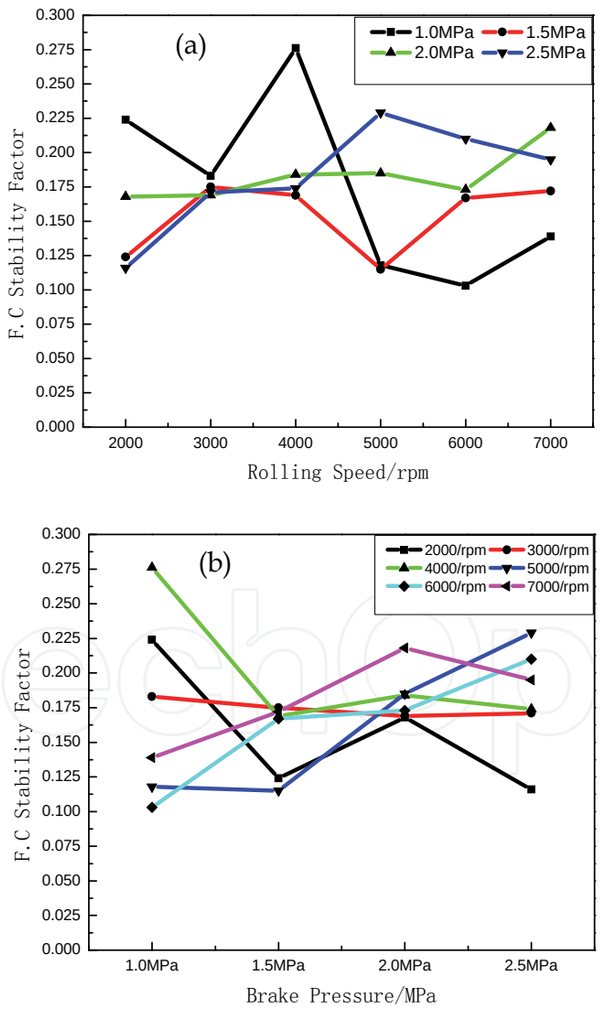

Fig. 10. The relation between the stability factor of friction coefficient and the brake pressure as well as the rolling speed

From the Figure 10(a), it can be seen that friction coefficient stability decreased with the increasing rolling speed under 1.0MPa brake pressure, but slightly increased under 1.5MPa, 2.0MPa, and 2.5MPa brake pressure condition. The reason is that the abrasion in low rolling speed and low pressure is abrasive grain wear as the main. The spalled pieces were squeezed and rolled on the friction surface, leading to the weak friction coefficient stability. However, with the increasing rolling speed, the adhesive wear became the main abrasion instead of the grain abrasion as the main. The phenomenon of friction coefficient decreasing emerged, resulted in the friction coefficient fluctuation decrease.

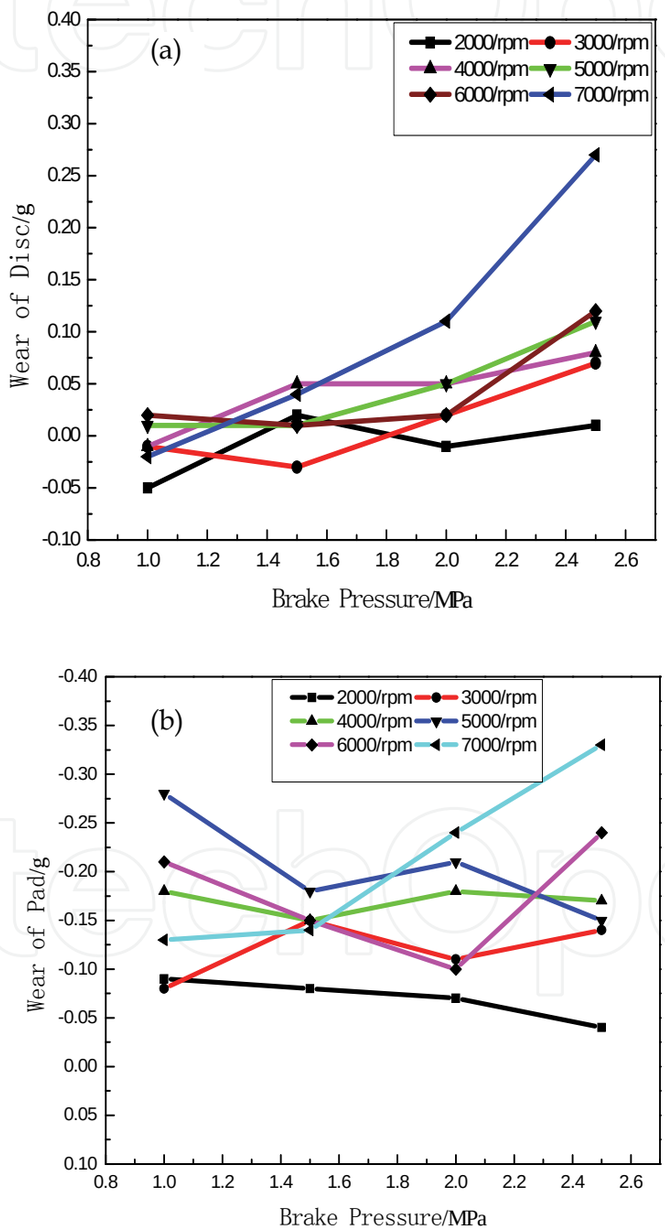

Fig. 11. The relation between the wear and the brake pressure in both disc and pad

Figure 10(b) indicated that the abrasion in lower rolling speed (2000rpm, 3000rpm, and 4000rpm) situation, is abrasive grain abrasion as the main. While the brake pressure increased, the rolling spalled pieces were easy to be squeezed, leading to the decrease of friction coefficient fluctuation. However, while the brake pressure increased further, the great amount of adhesive wear emerged, leading to the stability of the friction coefficient. In higher rolling speed situation, the friction surfaces were damaged severely with the increasing brake pressure and further adhesive abrasion. Therefore, the friction coefficient fluctuation was amplified.

Figure 11(a) shows the wear variation of SiC-5120 steel with various rolling speed, as brake disc. In lower rolling speed situation, with the increasing brake pressure, the mass of the encountered peer brake material adhered to the friction surface increased, but the adhering process kept slow. However, the adhesion mass increased aggressively in 7000 rpm situation.

Under the same rolling speed, the more brake pressure, the more damage in the friction surface and the more wear emerged. In lower rolling speed situation, the abrasion is grain abrasion and adhesive wear as the main, and the adhesive wear compensated the loss led by grain abrasion. Therefore, the mass increasing on friction surface is not much. However, the adhesion dominated the abrasion in 7000rpm situation, the great amount of friction energy welted the friction surfaces of disc (SiC-5120 steel) and pad (SiC-copper). The more brake pressure, the more friction energy was generated. Since the melting point of copper is far lower than that of steel, more pad material were welted to the disc.

5. References

Bauer H., Li L. (2005). *Foreign Locomotive & Rolling Stock Technology*, China Railway Publishing House, Beijing.

Desplanques Y., Degallaix G., Copin R., Berthier Y. (2001). A tribometer for the study of materials under railway braking conditions. *A Tribometer for the Study of Materials under Railway Braking Conditions*, Vol. 39, pp. 389-91.

Guérin J. D., Bricout J. P., Laden K., Watremez M. (1997). High thermal diffusivity materials for railway brake discs. *Tribology Letter*, Vol. 3, pp. 257-67

Kang, H.K., Kang, S. B. (2006). Thermal decomposition of silicon carbide in a plasma-sprayed Cu/SiC composite deposit. *Materials Science and Engineering: A* Vol.428, pp. 336-345

Lide D.R. (2009) *Handbook of Chemistry and Physics*, CRC Press/Taylor and Francis, Boca Taton.

Rado, C., Drevet B. (2000). The role of compound formation in reactive wetting: the Cu/SiC system. *Acta Materialia* Vol.48, pp. 4483-4491.

Tirovic M., Ali G. (2001) Design synthesis of non-symmetrically loaded high-performance disc brakes Part 1. *Proceedings of the Institution of Mechanical Engineers, Part F: Journal of Rail and Rapid Transit.* Vol. 215, pp. 101-9

Wahlström J., Olander L., Olofsson U. (2010). Size, Shape, and Elemental Composition of Airborne Wear Particles from Disc Brake Materials. *Tribology Letter.* Vol. 38, pp. 15-24.

Zhang S., Li Y., Qu S., Chen W. (2010) Friction and Wear Behaviour of Brake Pads Dry Sliding Against Semi-Interpenetrating Network Ceramics/Al-alloy Composites. *Tribology Letter*.Vol. 38, pp. 135-46.

Zhang L., Qu X., Duan B., He X., Ren S. (2008) Microstructure and thermo-mechanical properties of pressureless infiltrated SiC_p/Cu composites. *Composites Science and Technology*. Vol.68, pp.2731-2738.

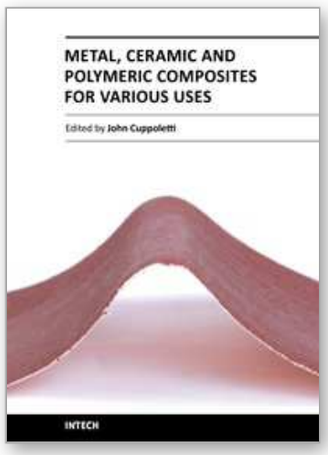

Metal, Ceramic and Polymeric Composites for Various Uses

Edited by Dr. John Cuppoletti

ISBN 978-953-307-353-8
Hard cover, 684 pages
Publisher InTech
Published online 20, July, 2011
Published in print edition July, 2011

Composite materials, often shortened to composites, are engineered or naturally occurring materials made from two or more constituent materials with significantly different physical or chemical properties which remain separate and distinct at the macroscopic or microscopic scale within the finished structure. The aim of this book is to provide comprehensive reference and text on composite materials and structures. This book will cover aspects of design, production, manufacturing, exploitation and maintenance of composite materials. The scope of the book covers scientific, technological and practical concepts concerning research, development and realization of composites.

InTech Europe
University Campus STeP Ri
Slavka Krautzeka 83/A
51000 Rijeka, Croatia
Phone: +385 (51) 770 447
Fax: +385 (51) 686 166
www.intechopen.com

InTech China
Unit 405, Office Block, Hotel Equatorial Shanghai
No.65, Yan An Road (West), Shanghai, 200040, China
中国上海市延安西路65号上海国际贵都大饭店办公楼405单元
Phone: +86-21-62489820
Fax: +86-21-62489821

IntechOpen